Earthquake Engineering, Tenth World Conference © 1992 Balkema, Rotterdam. ISBN 90 5410 060 5

Cyclic undrained shear behavior of sand under surface wave stress conditions

T. Sugano & E. Yanagisawa
Tohoku University, Sendai, Japan

ABSTRACT: The liquefaction phenomenon during earthquake excitation is one of the serious problems in earthquake engineering. Generally, the liquefaction analyses are based on the multiple reflection theory of S wave, and these analyses are commonly used for the design of structural foundations. Some examples of damage due to liquefaction can be explained by surface wave responses, however, the effects of surface waves on cyclic undrained deformation behavior of sands are not so well understood. In this paper, the cyclic undrained deformation characteristics of sands subjected to the stress condition which is produced by Love wave or Rayleigh wave during an earthquake are focused. In the experiments, the condition of sand specimens are carefully prepared to realize particle structures in natural sand deposit. In order to investigate the cyclic undrained shear behavior of sands, two experimental apparatuses are used. One is a hollow cylindrical torsional shear apparatus used for the case of principal stress axes rotation as Rayleigh wave propagation condition and the other is a newly designed bi-axial shear apparatus used to simulate Love wave propagation condition.

1 CYCLIC UNDRAINED SHEAR BEHAVIOR OF SANDS UNDER RAYLEIGH WAVE PROPAGATION CONDITION

The stress and strain conditions of an element in the ground during Rayleigh wave propagation are shown in Fig.1, where the direction of Rayleigh wave propagation is assumed to be in the X_1 axis. The stress condition of a sand sample is illustrated in Fig.2. The angle β is defined as the angle between the direction of the major principal stress axis and the vertical direction of a specimen. The definition of a ratio of the shear stress(b) to the deviatoric stress(a) is shown in Fig.3. To realize these stress conditions in a laboratory test, the hollow cylindrical torsional shear apparatus is adopted for the experiments. The stress condition in an element during Rayleigh wave propagation is calculated by the elastic theory(Fig.4) which shows the stress ratio a/b change with the depth. The stress paths of undrained cyclic shear tests in the present study; i)β-fixed undrained cyclic loading tests and ii)b/a-fixed undrained elliptic shape stress path loading tests are shown in Fig.5.

1.1 *Specimens*

Toyoura sand (G_s=2.622,e_{max}=0.947, e_{min}=0.579) whose particle shapes were observed to be in the range of angular to sub-angular shapes is used for all the experiments. The specimen (H=250mm, Ri=100mm, Ro=125mm, Dr=55±3%) is prepared by MSP method(Miura et al. 1982), which causes strong anisotropy in their fabrics and mechanical properties due to the parallel alignment of subelongated sand particles as like as a natural sand deposit. In undrained cyclic loading tests, a backpressure of 2.0kgf/cm^2(196kN/m^2) and an isotropic consolidation pressure of 2.0kgf/cm^2(196kN/m^2) are applied to the specimens.

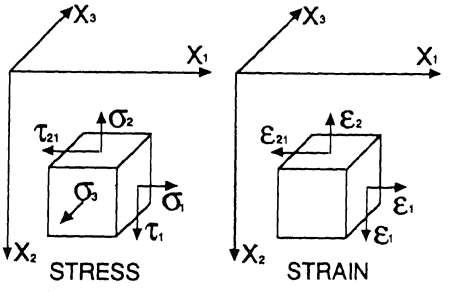

Fig.1 Stress and strain components of Rayleigh wave

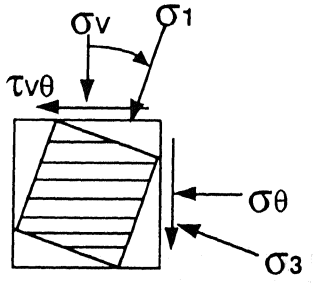

Fig.2 Stress condition of a specimen

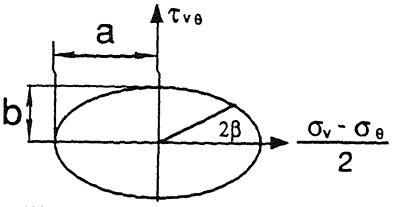

Fig. 3 Definition of a and b

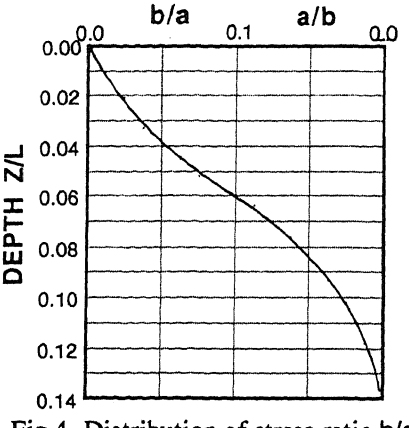

Fig.4 Distribution of stress ratio b/a

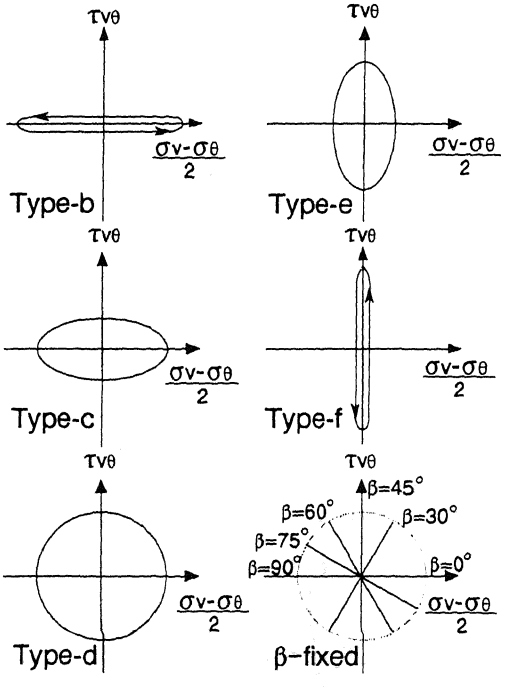

Fig. 5 Stress paths

1.2 *Experiments*

i) β-fixed cyclic undrained loading test: To investigate the inherent anisotropy of the specimen, cyclic undrained tests were carried out keeping the angle of the major principal stress axis βi to 0(triaxial shear), 30, 45(torsional shear), 60, 75 and 90(triaxial shear) degrees, respectively. The relationships between the direction of initial loading(β_i) and the number of cycles to cause 2.5% single amplitude shear strain is shown in Fig.6. If the liquefaction strength is defined as stress ratio at 2.5% single amplitude shear strain, a kind of liquefaction resistance which varies with the initial loading direction(βi) as shown in Fig.6.

During cyclic undrained loading, we can obtain the energy dissipation as eq.(1)

$$dW = \sigma_v d\varepsilon_v + \sigma_r d\varepsilon_r + \sigma_\theta d\varepsilon_\theta + \tau_{v\theta} d\gamma_{v\theta} \quad (1)$$

Normalized by effective mean stress p' yields the increment of a state parameter Ss (Moroto 1976),

$$dSs = dW / p' \quad (2)$$

Then accumulate eq.(2) gives the Ss

$$Ss = \int dSs \quad (3)$$

Fig.7 shows the normalized energy dissipation calculated by eq.(3) convined with Fig.6. Fig.7 indicates that the values of Ss at the initial liquefaction occurrence are almost same.

ii)b/a-fixed cyclic undrained elliptic shape stress path loading tests: The elliptic stress paths selected for the experiments are shown in Fig.5, where the amplitude of maximum shear stress is the same in each stress path.

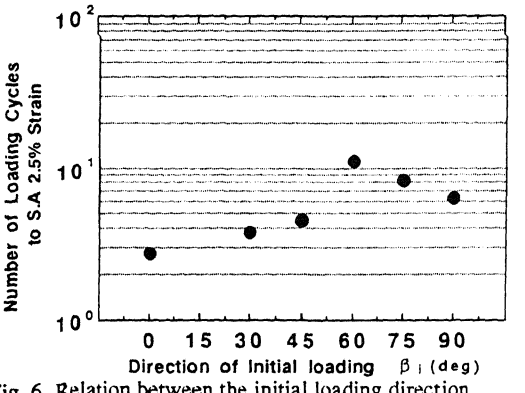

Fig. 6 Relation between the initial loading direction and the number of loading cycles to S.A. 2.5% strain

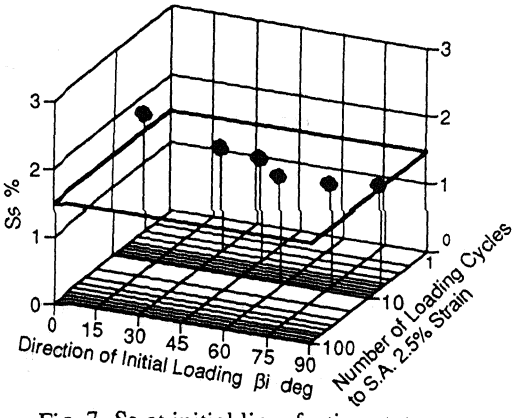

Fig. 7 Ss at initial liquefaction state

Typical effective stress paths in the case of Type-d(b/a=1), Type-c(b/a=0.5) and Type-e(b/a=2) are shown in Fig.8(a),(b),(c) respectively.

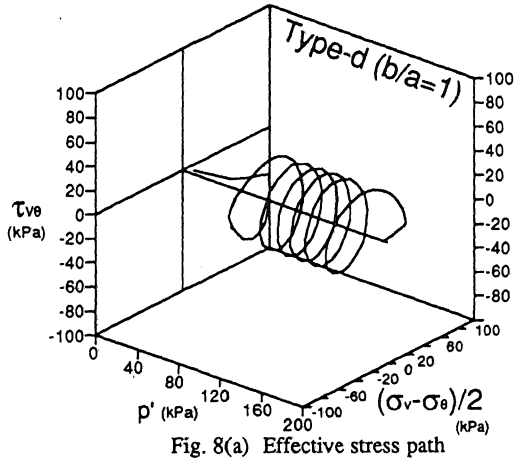

Fig. 8(a) Effective stress path

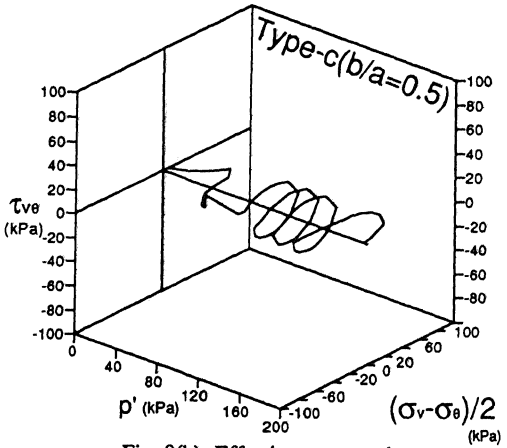

Fig. 8(b) Effective stress path

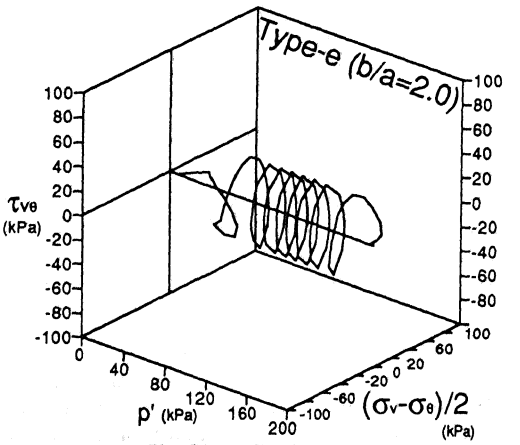

Fig. 8(c) Effective stress path

The relationships between cyclic shear stress ratio and the number of cycles to cause 2.5% single amplitude of shear strain are shown in Fig.9. The liquefaction resistances depend on the shape of stress paths. For a given number of cycles the stress ratio required to cause liquefaction increases in the order of Type-d(b/a=1), Type-c(b/a=0.5), Type-b(triaxial shear), Type-e(b/a=2) and Type-f(torsional shear) of stress paths. Generally, the liquefaction resistance is examined by the conventional triaxial apparatus. However, as shown in Fig.9, it must be noted that the liquefaction resistances due to principal stress axes rotation are lower than those of due to triaxial condition.

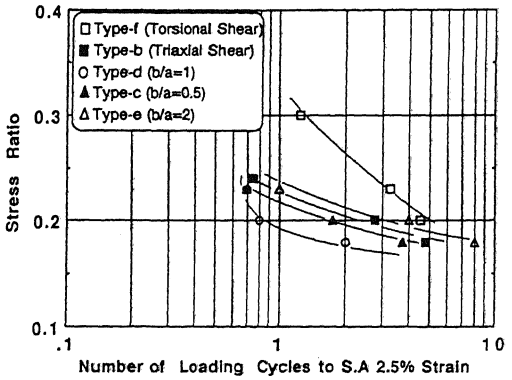

Fig. 9 Comparisons of cyclic stress ratio vs. number of loading cycles to S.A. 2.5% strain

Fig.10 shows the Ss at the initial liquefaction occurrence as mentioned previous section, also, the same manner as Fig.7.

Fig.7 and Fig.10 present that the value of Ss at the initial liquefaction occurrence defined by eqs.(1),(2),(3) is not affected by the anisotropy of specimen, the direction of stress path, the shape of stress path and the condition of principal stress rotation. So, Ss can be seen a kind of index of liquefaction occurrence.

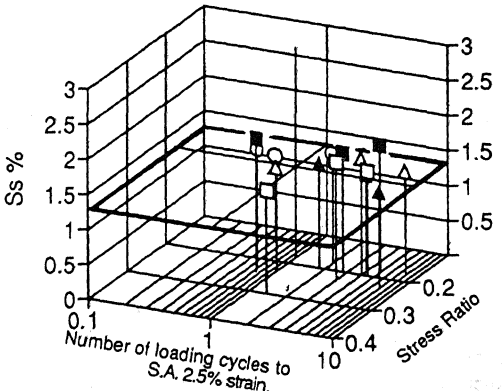

Fig. 10 Ss at initial liquefaction state

2 CYCLIC UNDRAINED SHEAR BEHAVIOR OF SAND UNDER LOVE WAVE PROPAGATION CONDITION

Fig.11 shows the definition of stress components in a soil element under Love wave propagation condition. This stress condition is expressed by stress and strain matrices which have the forms of Eqs.(4)and (5). Eqs.(6) and (7) are defined by the equivalent shear stress and equivalent strain, respectively.

$$\begin{bmatrix} \sigma_{11} & \tau_{12} & \tau_{13} \\ \tau_{21} & \sigma_{22} & \tau_{23} \\ \tau_{31} & \tau_{32} & \sigma_{33} \end{bmatrix} = \begin{bmatrix} \sigma_h & 0 & \tau_h \\ 0 & \sigma_v & \tau_v \\ \tau_h & \tau_v & \sigma_h \end{bmatrix} \quad (4)$$

$$\begin{bmatrix} \varepsilon_{11} & \varepsilon_{12} & \varepsilon_{13} \\ \varepsilon_{21} & \varepsilon_{22} & \varepsilon_{23} \\ \varepsilon_{31} & \varepsilon_{32} & \varepsilon_{33} \end{bmatrix} = \begin{bmatrix} 0 & 0 & \gamma_h/2 \\ 0 & \varepsilon_v & \gamma_v/2 \\ \gamma_h/2 & \gamma_v/2 & 0 \end{bmatrix} \quad (5)$$

$$\tilde{\tau} = \sqrt{\tau_v^2 + \tau_h^2} \quad (6) \qquad \tilde{\gamma} = \sqrt{\gamma_v^2 + \gamma_h^2} \quad (7)$$

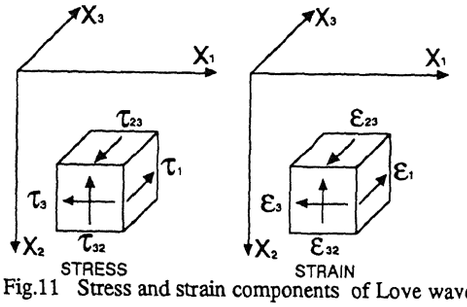

Fig.11 Stress and strain components of Love wave

2.1 *Test apparatus and specimens*

Fig.12 shows the bi-axial shear apparatus which is designed to apply stress condition discussed in above. A cubical specimen is placed in the middle of the apparatus.

In this study Toyoura sand is also used. The physical properties were measured to be G_s=2.621,e_{max}=0.926 and e_{min}=0.593. Specimens were prepared by pluviating the air-dried soil sample. In a cyclic undrained shear test, a back pressure of 0.5kgf/cm² (49kN/m²) and an effective vertical stress of σ_v'=0.5kgf/cm²(49kN/m²) are applied. The relative density Dr of consolidated specimens is 61+3%.

2.2 *Experiments*

From the theory of Love wave propagation, it can be easily recognized that the shear stress ratio τ_v/τ_h decreases as the depth increases. To carry out the experiment, we assume the model soil profile as shown in Fig.13. Shear stress distributions are calculated by the modified Haskell's method(Kamiyama 1975) under the condition of surface horizontal displacement applied

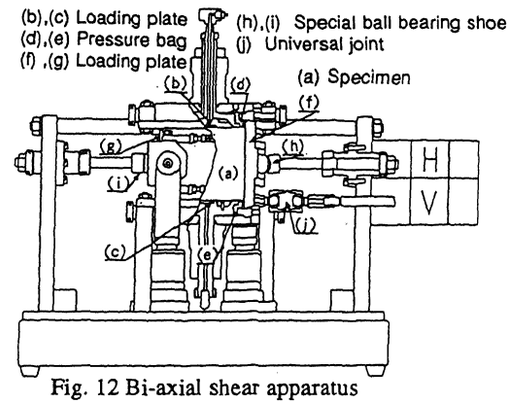

Fig. 12 Bi-axial shear apparatus

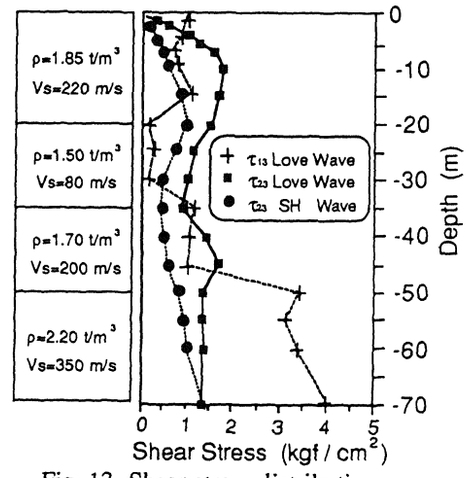

Fig. 13 Shear stress distributions

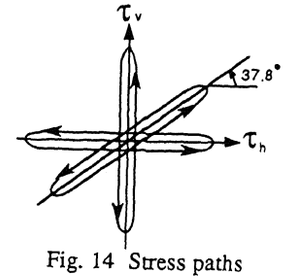

Fig. 14 Stress paths

by the sin-wave with the maximum amplitude of 5cm and the cycle of 1.41s. It is find that the magnitude of τ_{13} around surface region give larger values than τ_{23} calculated by S-wave analysis. Therefore undrained shear tests in different stress ratios are needed, which is shown by the different radial stress path in the τ_h-τ_v stress plane. Fig.14 shows three stress paths of cyclic undrained shear tests on the τ_h-τ_v stress plane carried out in the present study. These paths are i)H-direction; uni-axial τ_h shear test, ii)V-direction;uni-axial τ_v shear test and iii)VH-biaxial;τ_v/τ_h=0.78 (37.8 degree) shear test.

i)Uni-axial shear tests : Fig.15 shows the relationships between cyclic shear stress ratio and the number of cycles to cause 5% double amplitude shear strain for these three cases. It can be seen that the liquefaction resistance of the H-directional loading specimen is considerably greater than that of V-directional loading specimen. The difference of liquefaction resistance may be explained in the way that specimen has similar fabric to the natural fluvial sands.

ii)Bi-axial cyclic shear tests : The liquefaction resistance of Bi-axial cyclic shear tests is plotted in Fig.15. It can be seen in the figure that the liquefaction resistance locates between the values obtained by H and V-directional tests. For a fixed number of cycles N*, we can get stress ratios for the aforementioned three different directions. The shear stresses calculated from these three stress ratios can be plotted on the shear stress plane as shown in Fig.16. The locus of the equivalent shear stress can be regarded as an ellipse in which the ratio of the minor to major axes is approximately 0.67. This ellipse gives a kind of liquefaction resistance boundary for the specified number of cycles N*.

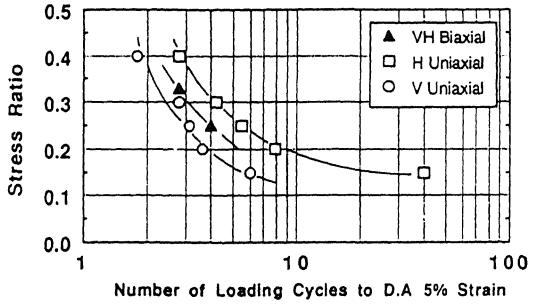

Fig. 15 Cyclic stress ratio vs. number of loading cycles to D.A. 5%

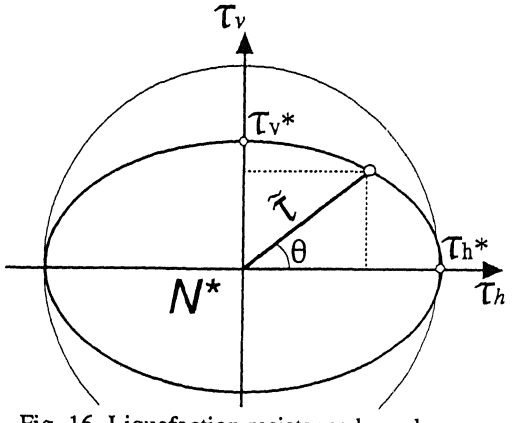

Fig. 16 Liquefaction resistance boundary

3 CONCLUDING REMARKS

From the results presented in this paper the following conclusions can drawn.

In case of Rayligh wave stress condition;

(1)The liquefaction resistance is affected by the inherent anisotropy of the specimen

(2)The liquefaction resistance is affected by the direction of stress path and the shape of stress path. Namely, in the case of principal stress axes rotation, the liquefaction resistances are lower than that of triaxial condition case.

(3)The normalized energy dissipation Ss at liquefaction occurrence is not affected by the inherent anisotropy of the specimen,the direction of stress path and the shape of stress path, even in the case of principal stress axes rotation.

In case of Love wave stress condition;

(1)It is pointed out that not only S wave propagation but also Love wave propagation may be a cause of liquefaction using a new designed bi-axial shear apparatus.

(2)The liquefaction resistance can be estimated by an elliptic boundary curve on the shear stress plane constructed with experimental data.

REFERENCES

Miura,S and Toki,S. 1982. A sample preparation method and its effect on static and cyclic deformation -strength properties of sand. *Soils and Foundations* Vol.22, No.1, pp.61-77.

Moroto,N 1976. A new parameter to measure degree of shear deformation of granular material in triaxial compression tests. *Soils and Foundations*, Vol.16, No.4, pp1-9.

Kamiyama, M. 1975. Stress and strain in ground during strong earthquakes. *Proc. of 4th Japan Earthquake Engineerin Symposium*, No.135, pp.273-280.